SmartMove: A Smartwatch Algorithm to Distinguish Between High- and Low-Amplitude Motions as well as Doffed-States by Utilizing Noise and Sleep

Marian Haescher, John Trimpop, Gerald Bieber, and Bodo Urban

Fraunhofer IGD, Joachim-Jungius-Str. 11, 18059 Rostock, Germany
{name.surname}@igd-r.fraunhofer.de

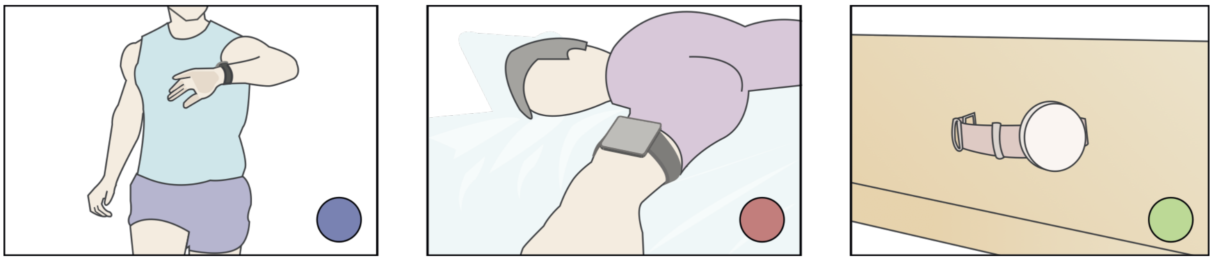

Figure 1: Detectable motion types: 1) high-amplitude motions (e.g. jogging, walking), 2) low-amplitude motions (e.g. heart rate, microvibration), 3) doffed. The colored dots indicate the cross reference to the detection states in Figure 2.

ABSTRACT
In this paper, we describe a self adapting algorithm for smart watches to define individual transitions between motion intensities. The algorithm enables for a distinction between high-amplitude motions (e.g. walking, running, or simply moving extremities) low-amplitude motions (e.g. human microvibrations, and heart rate) as well as a general doffed-state. A prototypical implementation for detecting all three motion types was tested with a wrist-worn acceleration sensor. Since the aforementioned motion types are user-specific, SmartMove incorporates a training module based on a novel actigraphy-based sleep detection algorithm, in order to learn the specific motion types. In addition, our proposed sleep algorithm enables for reduced power consumption since it samples at a very low rate. Furthermore, the algorithm can identify suitable timeframes for an inertial sensor-based detection of vital-signs (e.g. seismocardiography or ballistocardiography).

Author Keywords
Activity Monitoring; Activity Recognition; Wearables; Smartwatch; Microvibration; Sleep; Self Adapting; Seismocardiography; Ballistocardiography; Motion.

iWOAR '16, June 23 - 24, 2016, Rostock, Germany

ACM 978-1-4503-4245-2/16/06…$15.00
DOI: http://dx.doi.org/10.1145/2948963.2948964

ACM Classification Keywords
H.5.m. [Information interfaces and presentation]; J.3. [Life and Medical Sciences].

INTRODUCTION
With the proliferation of wearable devices and the fast-growing number of health services, detecting reliable vital signs is of high importance. Nevertheless, current wearable devices suffer of inaccuracy or critical motion artifacts in cases of measurements taken in unsuitable situations. Such sources of error, e.g. measuring while a device is mounted incorrectly, lead to erroneous and unreliable data. As a result of this, wearable measurement devices such as smartwatches should be able to evaluate critical states in which data validity cannot be guaranteed. Additionally, actigraphs in sleep science or fitness trackers for pulse detection are prone to detect sleep (ghost sleep) or pulse (ghost heart rates) in a doffed state. Avoiding this type of artifacts is crucial when feeding such data in important health-related services. In this paper, we contribute:

- An algorithm, which distinguishes between three motion intensities 1) high-amplitude motion, 2) low-amplitude motion, 3) doffed (see Figure 1)
- A Self-Adapting user dependent motion threshold
- An evaluation of the introduced sleep detection algorithm, which provides data for sleep analysis and Adaptation
- An evaluation of position dependency and over time effects of the sensor placement and mounting

RELATED WORK
Nowadays, wearable devices, such as smartwatches can also be used to detect various health related information. These information, contain vital parameters, such as heart rate

(HR), heart rate variability (HRV), respiration rate (RR), respiration rate variability (RRV), human microvibrations (MV), sleep related data, and several others. Since basic built-in sensors, such as accelerometers or gyroscopes, already provide a sufficient quality for recognizing the aforementioned data, standard consumer devices can be applied for medical or health-related applications [2].

High-Amplitude Motion
The term describes a strong motion that occurs globally (whole body) during human activity (e.g. walking, running), or locally in activities of daily living (e.g. at involved limbs while typing on a keyboard, or characteristic arm movements while eating in a sitting position). Subsequently, we present work that relates to high-amplitude motions.

Many research papers analyze the recognition of complex body motions and activities via accelerometers [2, 4, 9, 15]. Those papers always address strong motions that involve high values of g-force.

Low-Amplitude Motion
The term describes a tiny motion that is induced by vital functions of the human body (e.g. respiration, heart rate, microvibration). It is measurable at all body positions, in timeframes of global (whole body) or local inactivity. In the following we present related work in the area of low-amplitude motions.

Vital Data
Besides consumer devices, such as fitness trackers or smartwatches, many research projects focus on vital sign detection via novel wearable devices. Anliker et al. presented AMON: A Wearable Multiparameter Medical Monitoring and Alert System [1]. Besides such optical HR detection approaches, techniques as presented by Bieber et al. [2], or Hernandez et al. [10] present HR detection via wrist-worn SCG. In previous work, we investigated the performance of this measurement approach compared to commonly applied technologies (Haescher et al. [7]). Nevertheless, the aforementioned devices show sensor noise and also try to detect a HR even if the device is not worn, which can result in so called ghost heart rates [8].

Sleep Detection
Apart from position changes and short quick motions, sleep mostly consists of rest and inactivity (see Figure 3). Besides the polysomnography (PSG), which marks the gold standard in sleep science, wrist-worn actigraphs enable for a less obtrusive sleep detection. In addition, these devices are not fixed to a certain location, such as a sleep laboratory. Actigraphy devices utilize sleep scoring algorithms to distinguish between states, such as being awake or being asleep. Renown algorithms include the work of Mullaney et al. [12], Webster et al. [16], Cole et al. [5], Jean-Louis et al. [11], and Sadeh et al. [14]. The basic idea in the aforementioned papers is based on counting a weighted activity score. If the score exceeds a pre-defined threshold, wakefulness is detected and vice versa. Since the algorithms are based on activity scores (e.g. counting the number of zero crossings per accelerometer axis within a particular epoch), a continuous sampling is required. Furthermore, the algorithms do not allow for a distinction between 1) being worn while sleep or 2) being doffed. This leads to an incorrect or deficient sleep detection (ghost sleep).

Microvibrations
The human body is constantly moving, even in times of rest (e.g. while sleeping). Those tiny motions were reported first by Hubert Rohracher [13]. Rohracher detected continuously measurable motions of the muscles in endotherms. He also stated that compared to pathological tremor, which often vanishes in sleep, MV are always present. Furthermore, he reported changes in amplitude and frequency of the MV due to influences, such as temperature, medication, as well as physical or mental stress. He also reported a correlation or interference between MV and pulse, even though vibrations remained at animals after removing the heart. Gallasch et al. [6] measured MV at the upper limbs before and after stopping the blood flow via a blood pressure cuff. In contrast to Rohracher, who utilized piezoelectric phonograph pickups in his initial studies, Gallasch et al. applied accelerometers to measure the MV.

SMARTMOVE
Since the requirements for data validity in a medical context are extraordinary high, measurement artifacts need to be identified. This has to be done in order to ensure a high detection quality and to avoid critical misinterpretations.

We want to overcome these problems by introducing an algorithm capable of distinguishing between three types of motion 1) high-amplitude motion, 2) low-amplitude motion, 3) doffed. We encountered thus by applying the proposed algorithm several benefits can be achieved:

- A Simple and fast distinction between general activity, resting states, and a doffed device
- A Determination of suitable timeframes for sensing vital signs (e.g. accelerometer-based SCG)
- An Energy efficient and simple sleep detection algorithm to enable implicit adaptation of motion thresholds and dynamic adaptation to changes in detection over time or between individuals
- An Avoidance of noise-based artifacts due to measurements conducted while the device was doffed (e.g. ghost HR, ghost sleep, etc.)
- A Novel energy-saving mode, due to suspended vital data measurements during lengthy doffed periods.

Implementation
The basic idea of SmartMove is to make use of the human motions (e.g. MV and vital signs) to detect, if a device is actually worn and if so, which intensity of motion is present. Since the human body is constantly moving as shown by Rohracher [13], a distinction between being worn or being doffed is made possible. Therefore, a difference between the first state (doffed) and all remaining states (low- and high-amplitude motion) is characterized as a change in energy.

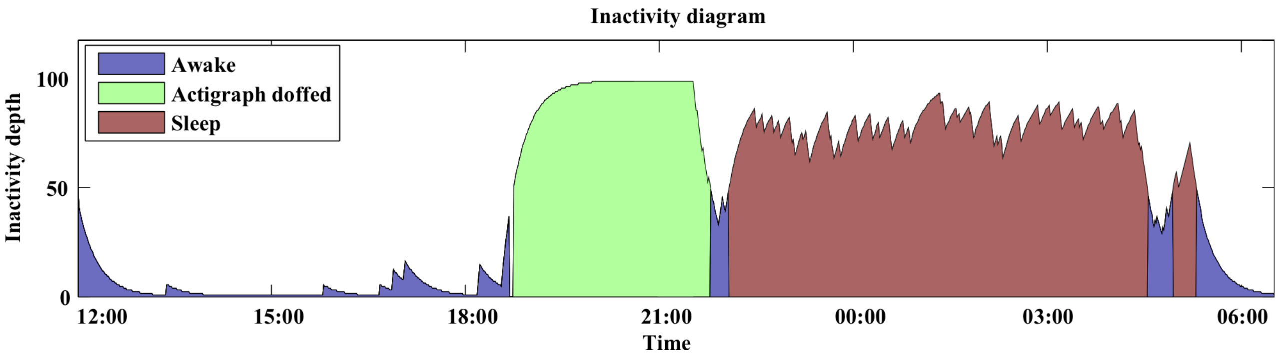

Figure 2: Graph of proposed sleep detection algorithm. Blue areas show wakefulness, green areas indicate that the device is not worn (doffed), whereas red areas indicate sleep. (signal smoothed with moving average)

For a discrete signal in time domain this concludes to:

$$E(a) = \sum_{n=0}^{N-1} |a[n]|^2 \tag{1}$$

Since the measured acceleration signal also contains noise and gravity, which can be identified as an offset in signal energy over time, the variation around the mean value is a good feature to analyze the different motion types. For this purpose, we computed the variance (see Equation 2). Since we applied a three-dimensional accelerometer, we computed the variance for each of the three individual axes separately to avoid calibration due to orientational dependencies. After each value was determined, we computed the mean variance for the three-dimensional signal (see Equation 3).

$$VAR(x) = \frac{1}{N}\sum_{i=1}^{N}(x_i\text{-}\mu)^2 \tag{2}$$

$$VAR_{3D} = \frac{(VAR_x + VAR_y + VAR_z)}{3} \tag{3}$$

The detection algorithm uses pre-trained thresholds to distinguish between the states 1) high-amplitude motion, 2) low-amplitude motion, 3) doffed.

Threshold Adaptation

We are convinced that the detection of vital data is performed best in an implicit manner. This means, that the user should not be forced to adjust or train the algorithms in order to perform reliably. As a result of this persuasion, we developed an algorithm (See Figure 4), which learns without explicit input or user-initiated training phases. To learn the individual thresholds for distinguishing between the previously proposed states, we selected three suitable training scenarios. To enable the distinction process, the doffed threshold has to be trained first since this information is needed for training low-amplitude motions. Therefore, the adaptation process is presented in the order of first determination.

Doffed Threshold

For the first scenario, we selected charging the watch, since this state enables for learning the sensor's individual noise level in a doffed state. After the device's power connecter was attached, we check for a homogeneous signal and start the doffed threshold training. A signal is considered as homogeneous if its max and min value are within the bounds of plus-minus four times the standard deviation added to the mean of the normed signal (see Equation 4, 5, 6).

$$Norm_{3D}(n) = \sqrt{{x_n}^2 + {y_n}^2 + {z_n}^2} \tag{4}$$

$$\max(\{x_1, x_2 \dots x_n\}) \leq 4 \cdot SD(Norm_{3D}) + M(Norm_{3D}) \tag{5}$$

$$\min(\{x_1, x_2 \dots x_n\}) \geq \text{-}4 \cdot SD(Norm_{3D}) + M(Norm_{3D}) \tag{6}$$

In case either the maximum or minimum is bigger or smaller than two times of its standard deviation threshold, the signal is inhomogeneous. In the consecutive training phase, we computed the per axis variance for a window size of 1024 samples. The devices sampling rate was set to 100Hz which led to a sampling time of 10.24 seconds.

Low-Amplitude Motion

For the second scenario, the device has to be worn during an activity that includes phases of low-amplitude motion. To ensure this requirement, we included a sleep detection algorithm (See Figure 2), since sleep mostly consists of low-amplitude motions. The algorithm scores inactivity by checking angular changes in sensor orientation in minutely transitions. This leads to a sampling rate of ca. 0.017Hz (once per minute). Since typical sleep detection algorithms also check for motion during the minute, their sampling rate is much higher (around 30Hz). This rate fits the purpose, since frequencies of 12Hz are sufficient for detecting human limb motion. In order to meet the Nyquist-Shannon theorem, a sampling rate of 24Hz is needed. Since our algorithm scores the motion as a change in position instead of high sampled motion scores, we can achieve similar results for lower sampling rates. This way, the devices can stay in low power modes for longer periods and thus save energy. If the angular change during a minutely transition exceeds a pre-defined threshold, the minute is scored as awake. To filter artifacts, we weighted the number of minutes awake in a defined timeframe to score an interval as asleep or awake. Based on the sleep detection, we algorithmically selected timeframes of homogeneous motion signals and trained the low-amplitude threshold by repeatedly computing the mean variance of the acceleration signal ($N = 1024$, $T = 10.24$s; $f = 100$Hz). The difference between an awake acceleration pattern versus a sleep acceleration pattern is visualized in Figure 3. The angular changes are computed as a difference between two vectors in three-dimensional space with the acceleration coordinates x, y, z. As seen in the following formula ($\vec{a}$ marks the vector of the previous minute, whereas $\vec{b}$ marks the vector of the current minute):

$$\cos\alpha = \frac{\vec{a} * \vec{b}}{|\vec{a}| \cdot |\vec{b}|}; \vec{a} = \begin{pmatrix} x \\ y \\ z \end{pmatrix}, \vec{b} = \begin{pmatrix} x \\ y \\ z \end{pmatrix} \tag{7}$$

High-Amplitude Motion

High amplitude motions are classified as motions that exceeded the trained low-amplitude threshold, or the measurement range of the applied accelerometer (+/- 2g in our setup). To define individual motion ranges and nuances, we also trained typical high-amplitude motion levels. This means that the mean variance level of high-amplitude motions is constantly adapted as the motion type occurs.

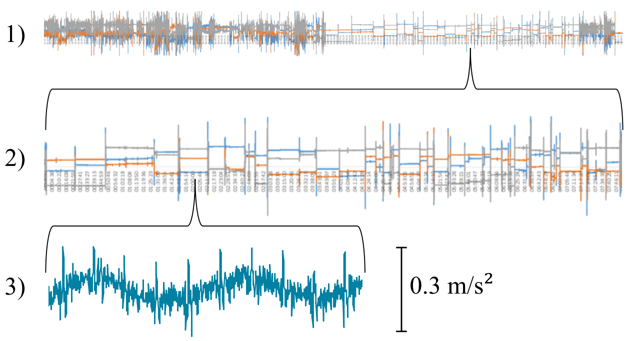

Figure 3: 3D-acceleration signal in m/s^2. Part 1) shows the signal for a whole day including mostly high amplitude motions, while part 2) shows mostly low-amplitude motions during the night. Part 3) shows a section of the x-axis with low-amplitude motions only.

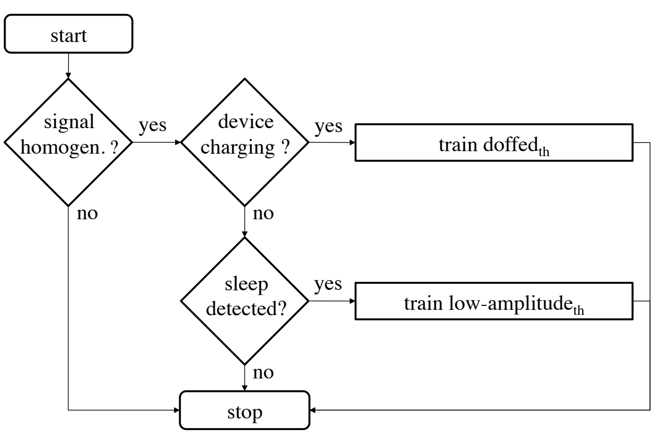

Figure 4: threshold training for detecting doffed-state and low-amplitude motion.

SLEEP STUDY

Since the sleep detection is a crucial part of the threshold adaptation module of SmartMove, we conducted a small study in a sleep laboratory to ensure its feasibility. The study involved measuring, seven subjects including six males and one female (mean age 56.4 +/- 11.4 yrs; mean height 173.6 +/- 6.3 cm; mean weight 100.43 +/- 17.9 kg; mean BMI 33.34 +/- 5.5). Every subject was undergoing a full polysomnography (PSG) while wearing an additional smartwatch, which was running three sleep algorithms. We evaluated our algorithm against a PSG and two well-established actigraphy algorithms introduced by Cole et al. [5], and Sadeh et al. [14]. Since the algorithms of Cole et al. and Sadeh et al. require a sampling rate of 25Hz, the raw-data was downsampled to a single value per minute (~0.017Hz) in case of our algorithm.

Comparison to Clinical Polysomnography

To compare our proposed sleep detection algorithm to a clinical PSG, we tested the detection of four parameters (Sleep onset latency – SOL; total sleep time – TST; sleep efficiency – SE; wake time after sleep onset – WASO). For each parameter, we conducted a one-way ANOVA analysis to detect if the results of our algorithm differ significantly in comparison to a clinical PSG. The results for the SOL ($F_{1,6} = 4.90$; $p = 0.0688$) show no significance between our proposed algorithm ($M = 14.43$; $SD = 14.81$) and the PSG ($M = 26.14$; $SD = 14.74$). In case of the TST ($F_{1,6} = 0.10$; $p = 0.763$), also no significance was found between our algorithm ($M = 278.00$; $SD = 51.63$) and the PSG ($M = 285.86$; $SD = 67.93$). The WASO results ($F_{1,6} = 0.37$; $p = 0.565$) for our algorithm ($M = 109.00$; $SD = 51.63$) showed also no significance in comparison with the PSG ($M = 93.57$; $SD = 64.31$). The same could be perceived for the SE ($F_{1,6} = 0.10$; $p = 0.763$) which also showed no significance by comparing our algorithm ($M = 0.7183$; $SD = 0.1334$) to the PSG ($M = 0.7386$; $SD = 0.1755$). In conclusion, our algorithm is comparable to a PSG approach.

Comparison to Actigraphy Algortihms

The results for our algorithm show a sensitivity of 81.10% and a specifity of 49.58%. The algorithm presented by Cole et al. scored a sensitivity of 71.66% as well as a specifity of 50.91, whereas the sensitivity of the algorithm presented by Sadeh et al. scored 82.55% and a specifity of 32.56%. To check the significance of our findings, we conducted a one-way ANOVA significance test. In case of the specifity, the test showed no significant differences ($F_{2,12} = 3.49$; $p = 0.0639$) between the algorithms of Cole et al. ($M = 50.90$; $SD = 24.32$), Sadeh et al. ($M = 32.55$; $SD = 19.35$), and our proposed algorithm ($M = 49.58$; $SD = 23.33$). In case of the sensitivity the test showed significance ($F_{2,12} = 4.54$; $p = 0.034$). A Tukey HSD test proved a significant difference ($p < .05$) between the algorithm of Cole et al. ($M = 71.65$; $SD = 22.84$) and Sadeh et al. ($M = 82.55$; $SD = 13.02$) in terms of Sensitivity. Our proposed algorithm showed no significant difference in terms of sensitivity ($M = 81.09$; $SD = 13.64$). In order to be complete, we computed the F-measure and accuracy (see Equations 8 and 9) for every algorithm to further evaluate the performance. The results show a F1-

score of 83.9 % in case of the algorithm proposed in this paper, whereas the algorithm of Cole et al. scored 79.4% as well as 80.2% for Sadeh's algorithm. The accuracy showed 71.4% and 70.5% for Cole's and Sadeh's algorithms, whereas our algorithm reached 76.2%.

$$F_1 = 2 \cdot \frac{precision \cdot recall}{precision + recall} \quad (8)$$

$$ACC = \frac{TP + TN}{TP + FP + FN + TN} \quad (9)$$

Results
We analyzed the performance and feasibility of the sleep detection algorithm presented in this paper, by comparing it to the golden standard of PSG as well as state of the art actigraphy algorithms. In case of the direct comparison with the PSG, none of the tested parameters (SOL, TST, WASO, SE) deviated significantly. The comparison of the proposed algorithm and two state-of-the-art actigraphy algorithms also showed no significant deviation. However, we found indicators, such as the F-measure and accuracy, that point out that our algorithm performed slightly better. A reason for this can be found in the discriminative power of the angle-dependent, minutely motion-detection feature that performed best compared to the weighed epoch feature applied in the algorithms of Cole et al. and Sadeh et al., which can be seen in the ROC-curve of Figure 5. Since the sampling rate in our approach is smaller by a factor of 1500, the acceleration sensor in a plain sleep detection scenario could stay in a low-power mode for a much longer duration. This enables the presented approach for reducing the overall energy consumption.

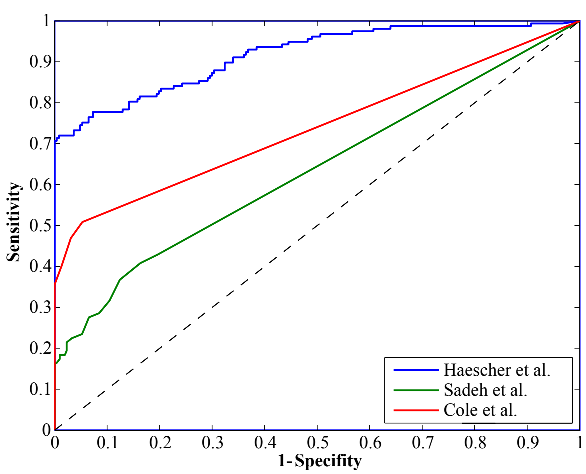

Figure 5: comparison of discriminative power for sleep scoring features. The farther the graph bends away of the diagonal, the better the discriminative power of the approach. Graph shows exemplary result of one subject (S06).

POSITION DEPENDENT SIGNAL ANALYSIS
In our general analysis, we intended to analyze mainly wrist mountings, since the proposed algorithm is developed for the use in smartwatches. Nevertheless, a smartwatch worn on the wrist can be placed on different parts of the human body. Since arm positions can vary in everyday scenarios, we designed a study to analyze the level of motion at different body positions. Besides the aforementioned fact such algorithms could also be integrated in other smart wearables, like smartpatches or smart jewelry. Therefore, a general analysis of low-amplitude motions on different body positions could be beneficial.

Study Design
5 subjects (4 males, 1 female; mean age 33.2 +/- 8.6 yrs; mean height 178 +/- 9.9 cm; mean weight 76 +/- 8.6 kg; mean body fat 18.08 +/- 5.2 %; mean BMI 24.0 +/- 1.5) participated in the study. Each subject had to lay on a bed, while staying as calm as possible. During the test a three-dimensional low-noise accelerometer (Shimmer 3 IMU) was placed on 15 body positions namely: 1) left and 2) right calf; 3) left and 4) right thigh; 5) left and 6) right chest; 7) neck; 8) left and 9) right temple; 10) left and 11) right upper arm; 12) left and 13) right wrist; 14) left and 15) right back of the hand (See Figure 6). We excluded the belly, since the motion at this particular body position is considered to be of a high amplitude (due to missing bone structure and strong respiratory movements).

In each scenario, the sensor was connected to the bare skin via a double-sided sticky tape. At each position, we conducted three consecutive measurements of a length of 10.24 seconds (equals 1024 samples at a sampling rate of 100Hz). This sums up to a total number of 225 measurements. We then calculated the variance for each window and computed the average for each body position.

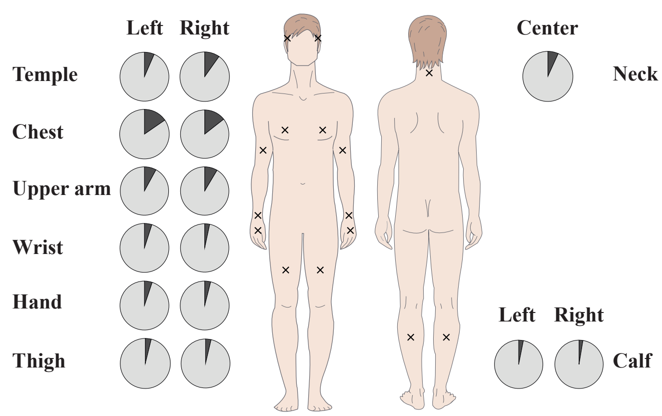

Figure 6: Sensor placements for position-dependent signal analysis. Pie charts show the variance measured at each position compared to the overall cumulative variance (all positions combined).

Results
Figure 7 shows the results of the measurements. Each body position shows a different level of motion and therefore a different level of variance. This effect is caused by the changing proximity to sources of excitement, such as the heart, lungs, or muscles. In addition, factors, such as varying tissue structure, BMI, state of health (e.g. mental stress, blood pressure etc.) influence the measurements. The

determined maximum average of the variance of all body positions was found to be VAR = 0.0029 m/s^2, whereas the overall minimum was found with VAR = 0.0005 m/s^2.

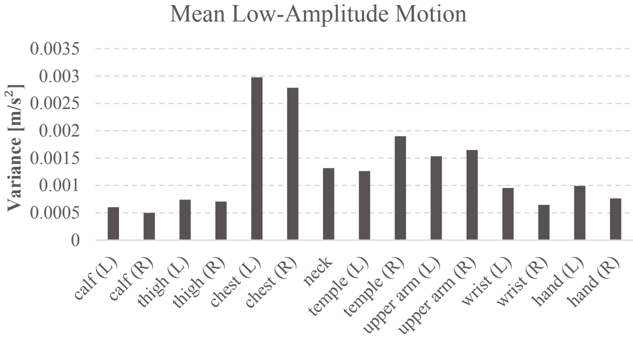

Figure 7: Position dependent average of variance (5 subjects; 15 body positions each).

OVER TIME SIGNAL ANALYSIS

In order to further analyze the different energy levels (doffed, low-amplitude motions, high-amplitude motions) over time, we tested three different attachments (glued to the wrist, wristband loosely mounted, wristband tightly mounted) as well as two body positions (see Figure 8) by using one sensor attached on one test subject. The single subject and single device study-design for the over time analysis was chosen in order to reduce the degrees of freedom (influencing variables, such as: specific sensor mountings, sensors level of noise or non-linearity, physiological characteristics).

Study Design

The subject had to lie down on a bed. During the measurement, the subject was advised to lie as calm as possible (trying to avoid even tiniest motions). To ensure that the subject had enough time to relax, the first five minutes where excluded from the measurement. After this phase of relaxation, the measurement started and data was collected for 20 consecutive minutes. In this timeframe, every 10.24 seconds a measurement was taken. The applied sampling rate was 100 Hz. This led to data windows of 1024 samples. Each data window was then used to compute the variance (as described in the aforementioned equations 2 and 3).

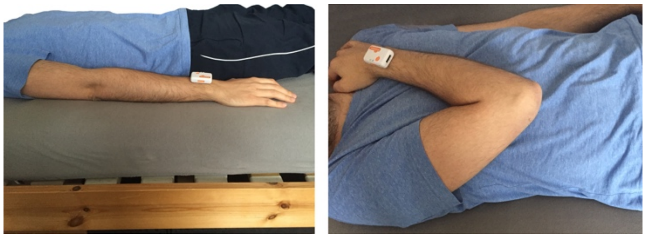

Figure 8: On the left, the wrist is resting beside the body whereas on the right, the wrist is resting on the subject's chest.

Doffed Measurement Over Time

For the initial measurement, the sensor (Shimmer 3 IMU) was connected to the charging dock while recording data in an empty room for 20 minutes. The resulting graph can be seen in Figure 9 (purple colored graph). The variance measured characterizes the deviation around the mean level of noise provided by the internal acceleration sensor (Kionix KXRB5-2042). According to the data sheet, the acceleration sensors root-mean-square noise level at 100Hz bandwidth was reported with 5.09 * 10^{-3} m/s^2.

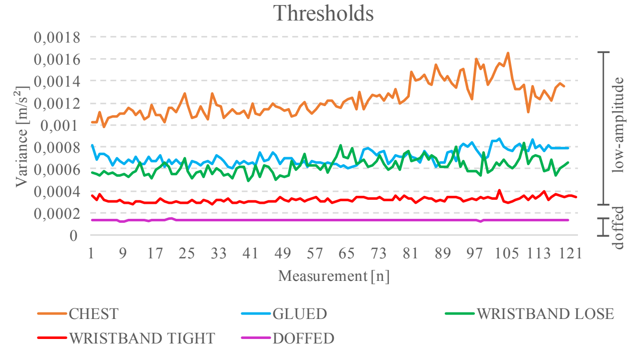

Figure 9: overview of all 20 minute measurements. The different mountings are marked by the blue, green, and red colored graphs. The doffed state is shown by the purple colored graph, whereas the measurement on the chest is marked by the orange colored graph.

Sensor Mounting Over Time

In order to analyze the sensor's variance over time while being worn, as well as the influence of the individual mounting (i.e. wristband or sticky tape), we performed three measurements with different mounting techniques. For the first measurement, we glued the sensor to the wrist by applying double-sided sticky tape. The resulting graph for the 20 minute measurement is shown in Figure 9 (blue colored graph). In the second test, we applied a wrist strap that was loosely mounted. The resulting graph can be seen in Figure 9 (green colored graph). In the last mounting scenario, we also applied a wrist strap, but mounted it very tightly. The resulting graph can be seen in Figure 9 (red colored graph). The measurements clearly indicate higher variance levels for all three mountings. This shows that a worn sensor can be clearly distinguished from a doffed sensor. Moreover, the tight mounting shows a lower variance level, since the movability of the sensor is reduced by the tight strap. As a result of this, a similar input energy (i.e. HR impulse) leads to a smaller deflection of the sensor. Nevertheless, the variance level of the tightly mounted sensor is continuously higher than the variance level of the doffed sensor.

Body Position Over Time

To check the level of variance over time in dependence on the body position, the sensor was placed on the chest. The resulting graph of the 20 minute measurement can be seen in Figure 9 (orange colored graph). Due to the fact that the chest is the source of the most energetic body movements in total rest (i.e. respiration or HR), the variance signal is clearly higher than all of the other measured signals of this test. Since motions such as the heart pumping blood through our vessels are induced here, we consider this position as an optimal place to measure the upper threshold for low-amplitude motions on the human body.

Results

The resulting thresholds of all scenarios tested over time can be seen in Figure 10. Based on the findings the low-amplitude motion range is defined as the lowest value of the wristband with tight mounting measurement (lower threshold; VAR = 0,000278 m/s^2) to the highest value of the wrist placed on the chest measurement (upper threshold; VAR = 0,00165 m/s^2). The doffed threshold is defined by the highest value of the doffed measurement (VAR = 0,000141 m/s^2). The influence of mounting tightness can be seen clearly by the drop in variance between a tightened (VAR = 0,000278 m/s^2) or loosened (VAR = 0,000491 m/s^2) wrist strap. The highest variance occurred during the test in which the wrist was resting on the subject's chest (VAR = 0,00165 m/s^2). All measurements that involved wearing the sensor on the body could clearly be distinguished (in terms of variance level) from the state in which the sensor was being doffed.

By comparing the results of this test to the results of the previously discussed position-dependent signal analysis (see Figure 7), a correlation between the low amplitude thresholds can be perceived. The overall minimum of the previous test showed a variance level of 0.0005 m/s^2, which fits perfectly in the observations made in this test. Solely, the average maximum variance was higher with 0.0029 m/s^2. We assume that this effect is caused by the mounting, since the results in Figure 7 relate to a sensor that was glued directly to the skin by using double-sided sticky tape, whereas the results in this test relate to a sensor glued to the wrist which was then placed on the chest (see Figure 8). Furthermore, the number of participants differs, which means the human factor in this test (body position over time; 1 subject) is much higher compared to the previously presented test (position dependent signal analysis; 5 subjects).

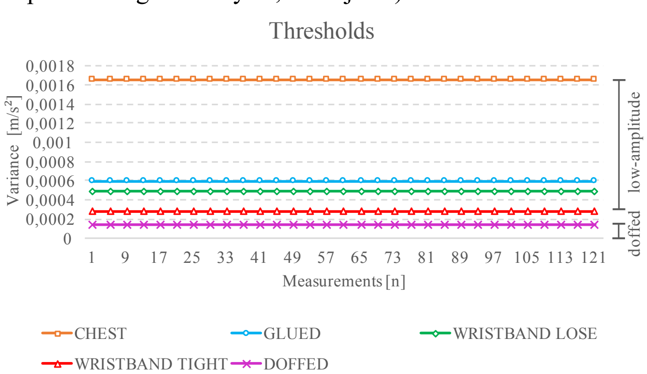

Figure 10: The resulting thresholds for all measured scenarios.

ENVISIONED SCENARIOS

By using our proposed algorithm and utilizing our threshold we achieve an improved activity, sleep, and vital data recognition. In the following, we describe scenarios, which could benefit from the outcomes of this paper.

Application other Wearable Devices

Besides smartwatches, our algorithm could be also applied to other wearables, such as smartpatches or smart jewelry. This way, the same benefits as mentioned in the sections before could be transferred to new device categories and wearing- as well as detection-scenarios.

Homogeneous Multi-Sensory Setups

Since accelerometer-based SCG is dependent on low-amplitude motions to detect valid parameters, a detection of such states would be mandatory. Nevertheless, the current level of motion can differ between the different limbs measured. In a homogeneous, multi-sensory wearable scenario with different wearing positions, our algorithm could detect which limb or body position is in a state of low-amplitude motion. This way, a valid detection of the specific sensor could be enabled.

Heterogeneous Multi-Sensory Setups

Optical heart rate detection techniques based on photoplethysmography (PPG) sensors can fail when not worn tightly, applied to inked or dark skin and consume significantly more power than accelerometer-based SCG or BCG approaches. This difference becomes crucial in a wearable scenario where battery performance is very limited. Nevertheless, PPG based approaches perform more reliably during high-amplitude motions. By detecting the current motion type, a system consisting of PPG and acceleration sensors represents the ideal detection technique for every situation (switch to optical sensing in case of high-amplitude motions or switch to inertial sensing during low-amplitude motions). This way, a high validity of data can be achieved while reducing the energy consumption of the wearable device.

Relaxation Measurement

Since low-amplitude motions are dominant during phases of relaxation, the duration and amplitude of the motion can be used to classify the current level of relaxation. Moreover, an additional vital-data measurement (e.g. accelerometer based SCG) could be enabled to further analyze the relaxation state.

Evaluation of Physiotherapy

Since the treatment of a physiotherapy cannot be evaluated in a proper way, the individual and subjective perception of each patient remains the measure for treatment quality. If health issues remain, the patient may evaluate the treatment with a negative bias. Since tensed and relaxed muscles provide a different movability of tissue, the variance at the same body position may change. By conducting a pre and post physiotherapy variance and SmartMoves low-amplitude threshold, a possible change in amplitude could be recognized to evaluate the quality of the treatment.

CONCLUSION

In this paper, we presented an algorithm to define dynamic thresholds that enable for a distinction between three general states 1) high-amplitude; 2) low-amplitude motion; 3) doffed motion. By constantly adapting those thresholds, a training to any individual wearing situation and user can be accomplished. This is possible due to the application of adaptation states, such as charging the device or sleeping while wearing the device. Since the proposed algorithm can be applied in a pre-filtering stage, artifacts that result from the device being doffed can be avoided. Furthermore, the algorithm detects timeframes of low-amplitude motions, thus enabling for choosing suitable vital-sign detection windows in SCG or BCG detection scenarios. As a byproduct, the algorithm enables for a low-power sleep detection. The results of the performed signal analysis showed that the algorithm works with a simple accelerometer. Every wearing scenario could be easily distinguished from being doffed. Nevertheless, the tests showed that the specific mounting as well as the body position the sensor is attached to have a strong influence on the resulting variance signal. These findings again underline the necessity of an adaptive and user-dependent threshold adaptation.

FUTURE WORK

In future work, we would like to analyze the algorithm's behavior in field tests on different customary devices. Furthermore, we like to investigate the acceleration amplitude for high and low-amplitude motions in an extensive study with more test subjects. Moreover, an analysis and definition of further states could be investigated. In future research, the use of additional sensor types, such as gyroscopes or magnetometers, could be taken into account. Moreover, we envision to test the possibility of reducing the energy consumption of PPG-based devices by initiating measurements based on the current motion state. This could include substituting PPG measurements by SCG approaches if possible. By doing this, we envision a further reduction of the energy consumed, especially in wearable scenarios.

ACKNOWLEDGEMENTS

This research is supported by the Federal Republic of Germany and the European Social Fund under the grants: BMWi/ESF 03EFFMV017; BMWi 16KN049121.

REFERENCES

1. Anliker, U., Ward, J. A., Lukowicz, P., Tröster, G., Dolveck, F., Baer, M., ... & Belardinelli, A. (2004). AMON: a wearable multiparameter medical monitoring and alert system. In *Transactions on Information Technology in Biomedicine*, 8(4), (pp. 415-427). IEEE.
2. Bao, L., & Intille, S. S. (2004). Activity recognition from user-annotated acceleration data. In *Pervasive computing* (pp. 1-17). Springer.
3. Bieber, G., Haescher, M., & Vahl, M. (2013, May). Sensor requirements for activity recognition on smart watches. In *Proceedings of the 6th International Conference on PErvasive Technologies Related to Assistive Environments (PETRA)*, (p. 67). ACM.
4. Bulling, A., Blanke, U., & Schiele, B. (2014). A tutorial on human activity recognition using body-worn inertial sensors. In *Computing Surveys (CSUR)*, 46(3), (p. 33). ACM.
5. Cole, R. J., Kripke, D. F., Gruen, W., Mullaney, D. J., & Gillin, J. C. (1992). Automatic sleep/wake identification from wrist activity. In *Sleep*, 15(5), (pp. 461-469).
6. Gallasch, E., & Kenner, T. (1997). Characterisation of arm microvibration recorded on an accelerometer. In *European journal of applied physiology and occupational physiology*, 75(3), (pp. 226-232).
7. Haescher, M., Matthies, D. J., Trimpop, J., & Urban, B. (2015, June). A study on measuring heart-and respiration-rate via wrist-worn accelerometer-based seismocardiography (SCG) in comparison to commonly applied technologies. In *Proceedings of the 2nd international Workshop on Sensor-based Activity Recognition and Interaction (iWOAR)*, (p. 2). ACM.
8. Haescher, M., Matthies, D. J., Trimpop, J., & Urban, B. (2016, May). SeismoTracker: Upgrade any Smart Wearable to enable a Sensing of Heart Rate, Respiration Rate, and Microvibrations. In *Proceedings of the 2016 CHI Conference Extended Abstracts on Human Factors in Computing Systems*, (pp. 2209-2216). ACM.
9. Haescher, M., Trimpop, J., Matthies, D. J., Bieber, G., Urban, B., & Kirste, T. (2015). aHead: Considering the Head Position in a Multi-Sensory Setup of Wearables to Recognize Everyday Activities with Intelligent Sensor Fusions. In *Human-Computer Interaction: Interaction Technologies* (pp. 741-752). Springer.
10. Hernandez, J., McDuff, D., & Picard, R. W. (2015, May). BioWatch: estimation of heart and breathing rates from wrist motions. In *Proceedings of the 9th International Conference on Pervasive Computing Technologies for Healthcare (PervasiveHealth)*, (pp. 169-176). IEEE.
11. Jean-Louis, G., Kripke, D. F., Cole, R. J., Assmus, J. D., & Langer, R. D. (2001). Sleep detection with an accelerometer actigraph: comparisons with polysomnography. In *Physiology & Behavior*, 72(1), (pp. 21-28). Elsevier.
12. Mullaney, D. J., Kripke, D. F., & Messin, S. (1979). Wrist-actigraphic estimation of sleep time. In *Sleep*, 3(1), (pp. 83-92).
13. Rohracher, H. (1964). Microvibration, permanent muscle-activity and constancy of body-temperature. In *Perceptual and motor skills*, 19(1), (pp. 198-198).
14. Sadeh, A., Sharkey, K. M., & Carskadon, M. A. (1994). Activity-based sleep—wake identification: an empirical test of methodological issues. In *Sleep*, 17(3), (pp. 201-207).
15. Ward, J. A., Lukowicz, P., Troster, G., & Starner, T. E. (2006). Activity recognition of assembly tasks using body-worn microphones and accelerometers. In *Transactions on Pattern Analysis and Machine Intelligence*, 28(10), (pp. 1553-1567). IEEE.
16. Webster, J. B. (1982, December). An activity-based sleep monitor system for ambulatory use. In *Sleep*, 5(4), (pp. 389-399).